One-Dimensional Edge Contacts to Two-Dimensional Transition-Metal Dichalcogenides: Uncovering the Role of Schottky-Barrier Anisotropy in Charge Transport across math xmlns="http://www.w3.org/1998/Math/MathML" display="inline" overflow="scroll">msub>mrow> mi>Mo/mi>mi mathvariant="normal">S/mi>/mrow> mn>2/mn>/msub>/math>/Metal Interfaces

Kamyar Parto, Arnab Pal, Tanmay Chavan, Kunjesh Agashiwala, Chao-Hui Yeh, Wei Cao, and Kaustav Banerjee

Phys. Rev. Applied **15**, 064068 — Published 28 June 2021

DOI: 10.1103/PhysRevApplied.15.064068

One-dimensional edge contacts to two-dimensional transition-metal dichalcogenides: Uncovering the role of Schottky-barrier anisotropy in charge transport across MoS_2/metal interfaces

Kamyar Parto, Arnab Pal, Tanmay Chavan, Kunjesh Agashiwala, Chao-Hui Yeh, Wei Cao, and Kaustav Banerjee*
ECE Department, University of California, Santa Barbara, CA; *Email: kaustav@ece.ucsb.edu

***Abstract*—** One-dimensional (1D) edge contacts to two-dimensional (2D) Transition Metal Dichalcogenides (TMDs), which offer unique features in the design of electronic devices have recently gained attraction. However, the physics of Schottky-barrier of the edge contacts and how exactly it differs from the conventional top-contacts is not well known. This paper presents a comprehensive ab-initio DFT-NEGF study of the electrical properties of edge contacts to 2D MoS_2. It is observed that, due to the intrinsic terminated edge-states, 1D edge contacts to MoS_2 are pinned more strongly to a charge-neutrality level that lies closer to the valence band and yields p-type characteristics, which are in contrast to top-contacts. This Schottky barrier anisotropy allows edge contacts in MoS_2 to outperform top contacts in p-type conduction, despite their atomically thin one-dimensional interfaces. Furthermore, the lower limits of contact resistance achievable by edge contacts to MoS_2 is estimated. The role of doping, different edge terminations, and Schottky barrier inhomogeneity in imperfect edge or hybrid contacts is analyzed to assess and provide design guidelines and conditions under which we can utilize the edge contacts for various applications.

I. Introduction

Since the successful exfoliation of monolayer 2D semiconducting Transition Metal Dichalcogenides[1] (TMDs) in 2005, a tremendous amount of research effort has been dedicated to this class of materials. 2D TMDs offer a plethora of intriguing capabilities and unique physics. Their monolayer (1L) forms have suitable direct bandgaps, high mobilities even at atomically thin body thickness, and relatively pristine dangling bond-free surfaces, which has made them the primary contender to replace Silicon in future transistor technology nodes[2–4], thin-film transistors[5], or potential stacked-3D integrated circuit architectures that promise to sustain Moore's law well beyond the foreseeable transistor scaling roadmap[6]. The strong spin-orbit coupling in combination with the unique spin-valley locking phenomena in 2D TMDs has revitalized the spintronics and valleytronic communities[7–10]. Exciting optoelectronic features such as tunable bandgaps[11], rich exciton physics[12,13], and the ability to host single photon emitters[14,15] has made 2D TMDs a fascinating research front in the photonics community. Bio-compatible label-free 2D TMD transistors with high surface to volume ratios have found application in biomedical[16] fields such as the design of highly-sensitive 2D biosensors[17]. While 2D TMDs continue to draw the attention of many researchers from a multitude of disciplines to the field, there are still a few fundamental challenges that need to be overcome to make 2D TMDs technologically relevant[18].

One such problem was, and still is, the question of "how to make low-resistance electrical contacts to 2D materials?" Metal-semiconductor contacts in nature tend to form Schottky barriers with rectifying behavior[19]. Although our knowledge of engineering TMD-Metal contacts for both charge[20–24] and

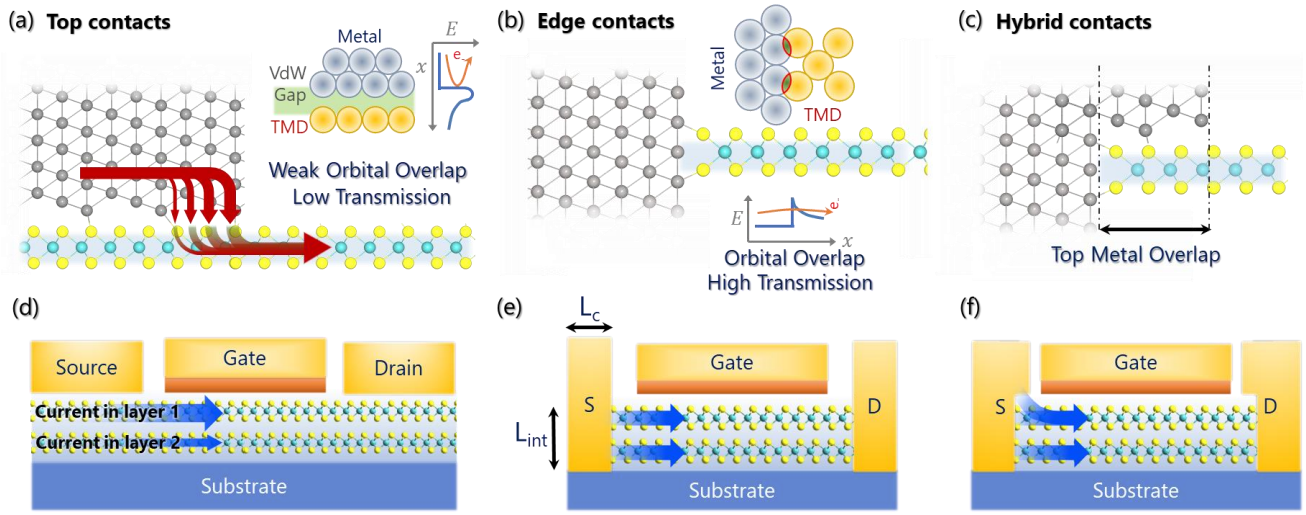

Fig.1. Possible geometries for metal-MoS_2 TMD contacts. (a) Conventional vdW top contacts. Red arrows denote the current trajectory, which is predicted to take place, for the most part, along the metal's edge. **(b)** Edge contacts. **(c)** Hybrid or impure Edge contacts. **(d)** Schematic of a bilayer 2D-FET with top contact. High anisotropy between in-plane and cross-plane conductivity increases the series resistance for the current path in lower layers. **(e)** Schematic of a pure edge contacted bilayer 2D-FET. Currents in both layers will be relatively equal since both layers are contacted at once. Also note that with the reduction of contact's physical length (L_C), the active interface area (L_{int}×W) will stay constant. **(f)** Schematic of a bilayer 2D-FET with Hybrid contacts.

spin[21,25,26] has undeniably progressed, contact resistance of today's conventional contacts to 2D semiconductors still exceeds that of their CMOS counterpart by at least an order of magnitude[27]. In conventional semiconductor technologies, Schottky contacts are engineered to become ohmic by strong doping of the semiconductor surface[28]. Unfortunately, due to their inherent thinness and fragility, 2D TMDs cannot be doped by standard, industry-friendly and scalable techniques like ion-implantation[23]. Other doping strategies[29] that have been explored so far, like in-situ substitutional doping, surface functionalization, and electrostatic doping, either are not suitable for large-scale manufacturing[23] or come with a penalty in device metrics such as high gate-source capacitances. Since a suitable doping mechanism is yet to be discovered, it becomes imperative to identify other "knobs" through which a Schottky barrier can be reduced. One of these knobs is the contact geometry.

2D materials can generally be contacted in two distinct geometries, namely top and edge contacts (**Fig.1a-b**). However, given the thinness of 2D flakes, it is readily apparent that even the best-case edge contacts may not be pure edge and can have some metal overlap on-top. We call this class of contacts impure edge contact or hybrid contacts. (**Fig.1c**). In most of the conventional top contacts (**Fig.1a**) to 2D materials, Metal atoms interact with the 2D semiconductor through weak van der Waals (vdW) interactions. This weak interaction is usually represented as a "tunneling barrier[20]" which adds additional width to the Schottky barrier and reduces the transmission probability of electrons (inset of Fig.1a). However, in contrast to top contacts, an edge metal contact (**Fig.1b**) covalently bonds with the 2D layer, resulting in a high orbital overlap without the additional vdW gap[20,30], and is predicted to achieve high transmission rates. These higher transmission rates are sometimes mistakenly construed to lower contact resistances in edge contacts. However, attributing the contact resistance solely to the width of the vdW tunneling barrier is a crude oversimplification. This is evident in the recent demonstrations of MoS_2 vdW transferred contacts[31], which despite the preservation of the vdW tunneling barrier, perform better than intimately deposited top contacts. It must be emphasized that the contact resistance is not only a function of the tunneling barrier but arises as an interplay between both the Schottky barrier height and transmission rates across the interface, in which the latter encompasses the effects of the vdW tunneling barrier. However, the problem becomes more complex since, as it will be discussed later, the Schottky barrier and tunneling barrier are also inter-dependent and cannot be tuned independently of each other. In most earlier research efforts on electrical contacts to 2D TMDs, barring from a few limited theoretical studies[20,21,32,33], edge contacts were often overlooked since (1) pure edge contacts are hard to fabricate and (2) the active area of the metal and semiconductor interface in edge contact is atomically thin compared to top contacts, thereby the current injection through them deemed to be limited.

However, in recent years, findings[34–37] have increasingly pointed out the importance and possible advantages of edge contacts. Firstly, 2D materials application can range from monolayer to few-layer bodies contingent on the functionality of the device. In few-layer devices, conventional top-contacts **(Fig.1d)** suffer from a high series resistance for vertical injection due to the highly anisotropic nature of 2D-layered TMDs which increases the cross-plane resistivity as the layer number increases. To overcome this, edge-contacts **(Fig.1e)** can be used to directly contact the buried layers in few-layer devices to improve performance. This method is especially advantageous in optoelectronics where the 2D material is encapsulated by *h*-BN layers for protection against the ambient and reduced substrate effects. Secondly, recent studies suggest that the current injection from top contacts to monolayer MoS_2 happens mostly at the edge of the metal and the conduction to the semiconductor under the metal is prohibited by the electrostatics of the system [35,36] (**Fig.1a,** red line denotes the current path with a transfer length of few angstroms). While the study of this effective edge-conduction requires more thorough experimental investigations, and the exact ratio of the edge and areal currents depends on the type of the metal, semiconductor, nature, and strength of metal-TMD atomic overlaps, and their biasing condition, its possibility raises a major conundrum. If in fact, electron injection in top contacts happens solely through an atomically narrow active area at the edge of the metal, then what performance advantages do top vdW contacts offer when compared to covalently bonded edge contacts?

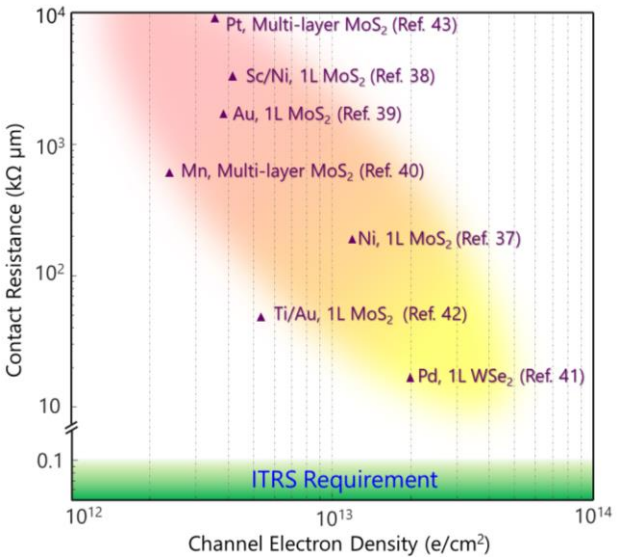

Fig.2. Edge contact demonstrations. Demonstrations of edge contacts have improved by over 4 orders of magnitude over the last years due to utilizing stronger gates and maturing of the fabrication techniques. Channel electron densities are extracted by $N = Cox\ (V_{GS}\text{-}V_{TH})/q$ where C_{ox} is the oxide capacitance, V_{GS} is the gate-source voltage, and V_{TH} is the threshold voltage. As expected, due to the reduction of the Schottky barrier's width at higher carrier concentrations, lower contact resistances can be achieved. Contact resistances, if not reported directly, were approximated by the slope of I_D-V_{DS} curves at the highest reported V_G normalized by width of the channel.

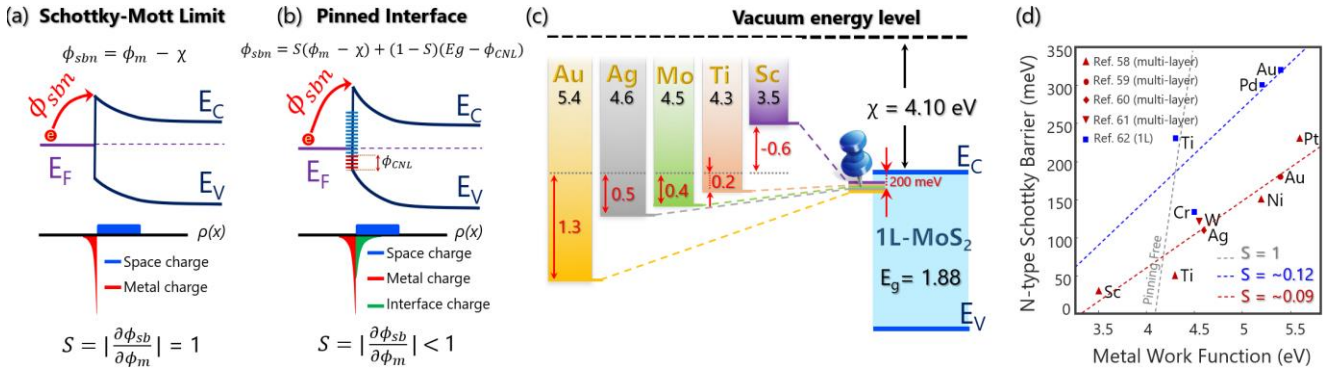

Fig.3. Fermi-level pinning in Schottky contacts. **(a)** Band-diagram of a hypothetical metal-semiconductor contact in the Schottky-Mott limit. n-type Schottky barrier is determined by the difference of metal's work function (ϕ_m) and semiconductor's electron affinity (χ). Bottom diagram shows the charge distribution across the junction. **(b)** In a realistic scenario where mid-gap interface states are present, charging of interface states can dominate the position of Fermi-level at the surface (See Supplemental Information 1). In this diagram, it is assumed that the Fermi-level lies above the Charge Neutrality Level (CNL), as it is the case for majority of conventional metals to MoS_2. In presence of interface states, sensitivity of the Schottky barrier to metal's work-function is decreased. **(c)** Band-alignment of several conventional top metal contacts with monolayer MoS_2. The difference between metal work function and MoS_2 electron affinity is indicated by the red arrows. These are the predicted Schottky barriers through the Schottky-Mott rule. However, in experiments, due to Fermi-level pinning, metal fermi-levels are instead pinned to a position approximately 200 meV under the E_c (follow dashed lines). **(d)** Schottky barrier height vs work function for both monolayer and multilayer MoS_2. Fermi-level pinning results in a decreased $|\frac{\partial \phi_{sb}}{\phi_m}|$ and is centered around the CNL. Note that the Schottky barriers of monolayer contacts are on average higher, which can be attributed to the larger band-gap of the TMDs at monolayer limit.

Despite these intriguing features of edge contacts, the electrical properties of edge contacts remain widely unexplored. Demonstrations of edge-contacts[37–44] are still in their infancy in terms of achieving acceptable contact resistances. Edge contacts to TMDs are typically fabricated in the same manner as edge contacts to graphene[45], which is achieved by utilizing *h*-BN encapsulation to isolate the semiconductor surface from the metal contact. An etching process is then utilized to cleave the 2D stack and expose the edge, which is then electrically contacted by a metallization process. Experimentalists have been trying to improve their contact resistances by utilizing ultra-high vacuum metal depositioning and in-situ Argon sputtering techniques to achieve sharper and cleaner junctions [37,42] close to the ideal. However, results still vary by orders of magnitudes (**Fig.2**). A clear picture of the physics and electronic dynamics of edge-contacts that can reveal their true potential is still missing. Exploration demands a holistic methodology to ascertain the value of different 2D contact approaches and their implications in various 2D device architectures.

In this study, taking MoS_2 as an example, we utilize a Density Functional Theory (DFT) coupled with Non-Equilibrium Green Function (NEGF) transport framework to study the electrical properties of lateral, top, and hybrid contacts to 2D MoS_2. The manuscript is organized as follows. First, the necessary physics and ab-initio framework used in the analysis is established in section. II. In Section. III, the edge-contact between 2H-MoS_2, and different 3D metals are studied using this method to investigate the effects of doping, interface geometry, Fermi-level pinning, and edge-termination on contact resistance (R_c). Moreover, the lower theoretical limits of edge-contact resistances to 2D MoS_2 are extracted and compared with conventional top contacts to identify the optimum design space of 2D lateral contacts. This section is concluded by discussing the effects of the Schottky barrier inhomogeneity on hybrid contacts. Finally, in Section IV, we provide an outlook by discussing the implications of the analysis on the future design of 2D devices, and examining the future necessary research directions.

II. METHODS

Physics of Schottky Barriers

The most important factor that governs the electrical property of any metal/semiconductor interface is the Schottky barrier. Schottky barrier for electron/hole is defined as the minimum energy from the Fermi-level required by electrons in the metal contact to overcome the energy barrier at the metal-semiconductor interface to reach the conduction/valence band of the latter (**Fig.3a**). Schottky barriers play a significant role in the design of 2D-FETs. Electrical characteristics of 2D-FETs at short channel lengths are dominated by their contacts and are usually modeled as two back-to-back metal-semiconductor Schottky diodes (known as the 2D-Schottky barrier FET model). Given the importance of the Schottky barriers, unfortunately, accurate modeling of Schottky barriers is still a challenging task. Formation of the Schottky barrier is not only dependent on the bulk electronic properties of the materials but also heavily relies on the detailed physics and chemistry of the interface, which usually becomes an untraceable problem due to the uncertainties and complexities involved.

Fortunately, many systematic trends still hold true, which provide insight into the physics of Schottky barriers. One of such trends and the cornerstone of any Schottky barrier model is the Schottky-Mott rule. The rule predicts that n-type Schottky barrier ($\phi_{sb\text{-}n}$) must follow, $\phi_{sb\text{-}n} = \phi_m - \chi$ relation,

i.e., the electron Schottky barrier is precisely proportional to the difference of metal's work function (ϕ_m) and semiconductor's electron affinity (χ) **(Fig.3a)**. This prediction grossly deviates from experimental results, which reveal that for conventional semiconductors such as Si and GaAs, barrier height weakly depends on the metal's work-function and is usually fixed at a value about 1/3 of the bandgap (referenced to valence band maxima) irrespective of the metal used[46]. The primary reason why the Schottky-Mott rule deviates from experimental trends lies in the interface or more specifically, the absence of any interface physics in the Schottky-Mott rule. When a metal comes into contact with the semiconductor, the atomic arrangement of the atoms at the interface is altered, chemical bonds are formed, and charge is redistributed into newly formed electronic midgap states that are a contribution from the orbital mixture in both metal and semiconductor. As a result, the Fermi-level at the interface, which determines the Schottky barrier, is now governed by the filling of the interface states rather than the bulk electronic bands as predicted by the Schottky-Mott relation **(Fig.3b).** In other words, Fermi-level becomes "pinned[46]" to an energy level that minimizes the surface charge, and the Schottky barrier becomes less sensitive to metal's work function **(Fig.3a-b).** This effect is captured through the S parameter definition, which determines the sensitivity of the Schottky barrier to the metal's work-function **(Fig.3b)**. In the absence of interface states, S=1 and Schottky-barrier becomes a function of the metal's work function. In the presence of a high density of interface states, S becomes negligible, and Schottky-barrier is determined by Charge Neutrality Level (CNL), irrespective of the work-function. CNL is the energy level at which the surface charge is minimized and is determined by the energy at which midgap states transition from donor-like to an acceptor-like nature[47]. In bulk semiconductors such as Si, the Fermi-level pinning problem is addressed by heavy doping of the contact regions, which makes the SB width vanishingly small or nearly transparent, leading to the realization of Ohmic contacts. We have dedicated supplementary Information 1 (See **SI.1** at [48]) to a quantitative semi-classical discussion of Fermi-level pinning, **SI.2** (see Supplemental Material in [48]) is dedicated to an atomistic picture, and for a more thorough analysis, readers are referred to the seminal papers by Tung *et al*. [49,50]

In 2D TMDs, the Fermi-level pinning haunts the electrical contacts to an even greater extent[21,23], especially in the absence of reliable doping techniques, the electrical response of most metal-TMD contacts are governed by their Schottky barriers. Conventional top contacts to 2D TMDs are dominated by a high concentration of defect states (D_{it}) at the surface. This mostly stems from the fact that the quality of 2D growth is still far from silicon technology. For instance, 2D MoS_2 surfaces that are theoretically supposed to be "pristine" or dangling bond-free regularly exhibit D_{it}'s in the order of 10^{11} to 10^{12} cm^{-2} contingent on their growth/exfoliation conditions[51]. While the atomic origin of these states is still under debate and has potentially been attributed to both S-vacancies[52–55] and transition metal defects[56], in MoS_2, they nevertheless introduce states with energies very close to the conduction band. To compensate for these defect states, the effective charge neutrality level moves close to the defect energy levels, and as a result[57], Fermi-level becomes pinned to these high-density defects and form n-type Schottky barriers with heights in the range of 50-200 meV[58–61] for multilayer and 100-350 meV[62] for monolayer MoS_2. **(Fig.3c-d).** Given the importance of Fermi-level pinning, several questions naturally come to mind. Firstly, where does the Fermi-level become pinned for lateral (edge) contacts? And how will it be different w.r.t the top contacts? The next question we address arises from the atomically thin interface area of lateral 1D interfaces. Does the atomically thin cross-section of the one-dimensional interface limit the minimum contact resistance, if so, what are the lower theoretical limits of 1D (edge) contacts?

To analyze the electrical properties of the lateral 1D interface and answer the aforementioned questions, an ab-initio transport framework is required to provide a quantitative picture of the band alignments, transmission probability of each available state, and finally, contact resistances for different contact configurations. In this study, we utilize an ab-initio DFT-NEGF transport framework using Synopsis QuantumATK[63,64]. Lateral interfaces of five conventional 3D metals (Sc, Ti, Mo, Ag, Au) with MoS_2 are analyzed. The chosen metals cover abroad range of work-functions (~ 3.5 to 5.2 eV) which allow us to probe further into the physics of Schottky barrier formation at these interfaces. Both n-type and p-type barrier heights are extracted at various doping levels for different metals. Electron transmission spectrums are extracted using NEGF formalism[65,66] and finally R_c is obtained through Landauer formalism to estimate the lower limits of contact resistance.
To introduce and justify our analysis method, we first apply it

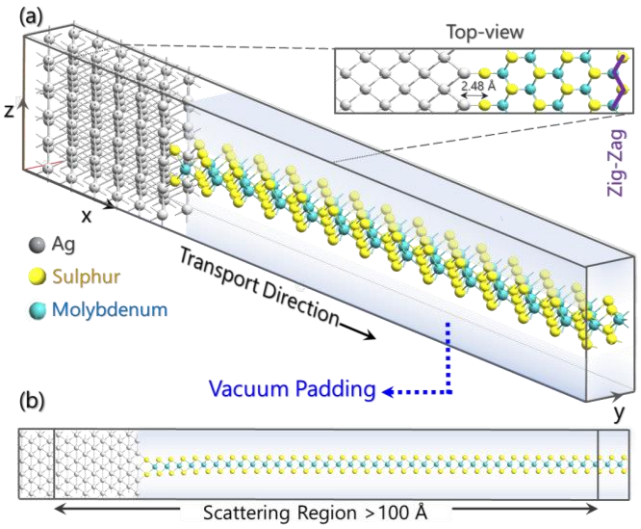

Fig.4. (a) Supercell geometry of DFT calculation. Note that the addition of ~ 7Å of vacuum padding is necessary to eliminate any interlayer coupling effects that QuantumATK may inadvertently induce by the repetition of the unit cell in the z-direction **(b) Two-electrode device used for NEGF simulations.** The length of the scattering region is chosen in accordance with doping levels to guarantee the screening of the interface potential.

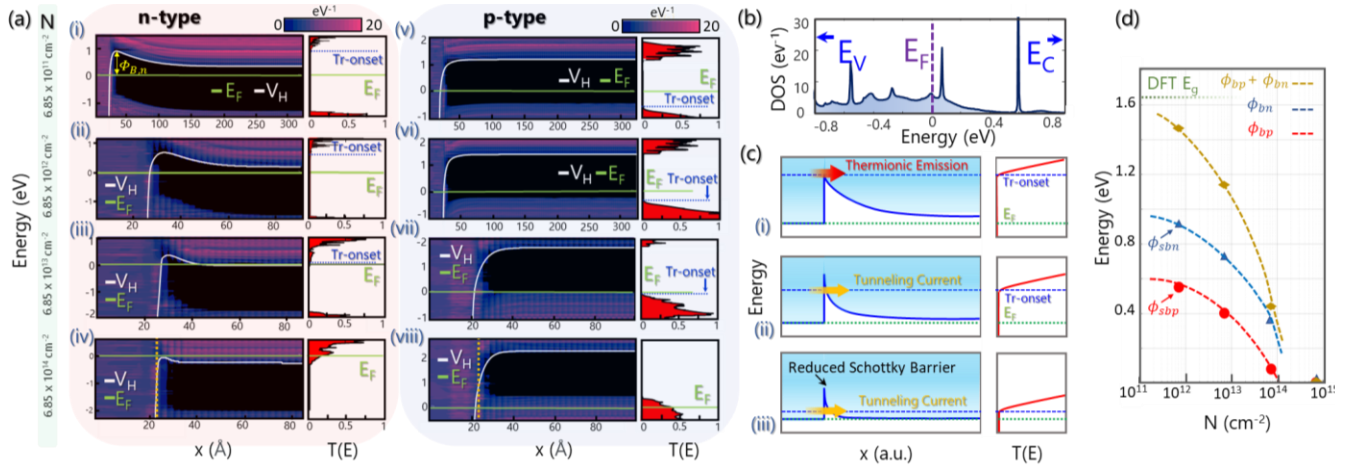

Fig.5. Schottky barrier extraction using DFT-NEGF for Ag-MoS_2 interface (a) Superimposed PLDOS, Hartree Potential, and Transmission Spectrum at various doping levels. (i) n-type 6.85×10^{11} cm^{-2} (ii) n-type 6.85×10^{12} cm^{-2} (iii) n-type 6.85×10^{13} cm^{-2} (iv) n-type 6.85×10^{14} cm^{-2} (v) p-type 6.85×10^{11} cm^{-2} (vi) p-type 6.85×10^{12} cm^{-2} (vii) p-type 6.85×10^{13} cm^{-2} (viii) p-type 6.85×10^{14} cm^{-2}. The white lines indicate the average Hartree potential $<V_H>$, which aids in the visualization of the band movements in the depletion zone. Note that at lower doping levels, due to the longer depletion regions, the length of the semiconductor side has been increased from 100 Å to 300 Å. The transmission spectrum is presented for each case in the adjacent box on the same energy scale. Barrier heights are read from the difference between E_F and onset of the transmission spectrum turn-on (Tr-onset). The yellow dashed lines in (iv) and (viii) denote the position of the metallurgical interface. **(b) Distribution of MIGs at the Ag-MoS_2 interface.** Projected Density of States (DOS) taken from the first and second row of MoS_2 atoms at the interface. Note that the density of the midgap states is higher towards the valence band. **(c) Relationship between the barrier height and the onset of transmission turn-on.** (i) At low doping, contacts are dominated by the thermionic emission. In such contacts, the onset of transmission corresponds one-to-one with the actual Schottky barrier. (ii) At intermediate doping, due to the thinning of the Schottky barrier width, electrons can tunnel through the barrier at energies lower than the Schottky barrier. Tr-onset will then deviate from the Schottky barrier. (iii) At very high doping levels, the Schottky barrier itself can be lowered by doping and further increases the mismatch between Tr-onset and actual barrier height. **(d) Barrier heights vs doping density:** As explained qualitatively in Fig.5.b and also quantitively in the SI.1 (see Supplemental Material at [46]), the barrier height will reduce as a function of doping. Therefore, we define the Schottky barrier height at the lowest possible doping where the n-type and p-type barrier sum up to 90% of the bandgap. This point is usually achieved at doping levels of about 10^{11} cm^{-2}, which is also close to intrinsic defect doping of most 2D TMDs.

to the Ag-MoS_2 interface as an example. One should note that this analysis method is not specific to only lateral 2D interfaces and can be used to analyze a variety of interfaces. DFT-NEGF calculations were performed using Perdew-Burke-Ernzerh (PBE) variant of Generalized Gradient Approximation (PBE-GGA) exchange-correlation functional[67], Hartwigsen-Goedecker-Hutter (HGH) pseudopotentials, 11×3×415 and 11×3×415 Brillouin zone *k*-point sampling for DFT and NEGF calculators, respectively, 240 Rydberg density mesh cut-offs and a 0.05 eV/Å maximum force constant for geometry optimizations. We further employed Grimme's DFT-D2 dispersion correction[68] to account for vdW interactions. GGA-HGH with DFT-D2 vdW correction setup has been previously identified to reproduce the experimental band structure and bandgap of MoS_2 (See **SI.3** available in Supplemental Material at [48]) reasonably well and has been widely used in the literature to probe the physics of TMDs. To avoid redundancy, **SI.4** (see Supplemental Material at [48]) is dedicated to the complete simulation results of all the other interfaces.

Next, a lateral interface between Ag <100> plane and MoS_2 zigzag (ZZ) Mo truncated interface with sulphur passivation **(**Mo-ZZ-2S) is constructed as seen in **Fig. 4.a**. Given the fact that MoS_2's edge has the lowest formation energy in Molybdenum zigzag terminated geometry with sulphur dimers (Mo-ZZ-2S)[69,70], we limit this study to the zigzag truncated interfaces. The metal plane orientation is chosen to allow us to construct supercells with low lattice mismatch and absolute strain (below 3%, with the entire strain applied to the metal to keep the semiconductor bandgap, and hence the Schottky barrier, unaffected) and are small enough to be computationally feasible. Next, the structure is geometrically relaxed, which allows for the formation of chemical bonds and any inevitable structural deformation as a result. Next, a two-electrode device is created for NEGF transport simulations (**Fig.4b**). An important requirement for the NEGF framework is that any built-in potential in the scattering region (either due to interface effects, defects, etc) must be sufficiently screened out before reaching the metal and semiconductor electrodes[66,71]. To satisfy this requirement, nine atomic layers of metals, sufficient to screen any interface effects on the metal side[20] are included in the scattering region. Similarly, the length and doping of the semiconductor region must be chosen sensibly to accommodate for the depletion width ($L > W = \sqrt{\frac{2\varepsilon_S V_{bi}}{qN_d}}$, where ε_s is the semiconductors dielectric constant, V_{bi} is the built-in potential, N_d is doping density, and q the elementary charge). In order to assess the effect of doping on contact resistance, MoS_2 is doped by rescaling the valence charge of individual atoms using atomic compensation charge method at eight different doping concentrations ($\pm6.85\times10^{11}$ cm^{-2}, $\pm6.85\times10^{12}$ cm^{-2}, $\pm6.85\times10^{13}$ cm^{-2}, $\pm6.85\times10^{14}$ cm^{-2}) with suitable semiconductor lengths (L>W) (300 Å, 300 Å, 100 Å,

and 100 Å respectively). Next, the Projected Local Density of States (PLDOS) of the system at different doping levels is calculated along the transport direction (x-axis), which gives an overall view of the band alignment of the metal-semiconductor contact. **Fig.5a** shows the PLDOS plots of the Ag-MoS_2 (Mo-ZZ-2S) interface at 8 different carrier concentrations. Moreover, to better visualize the band movements in the depletion region, the macroscopic in-plane average of Hartree Difference Potential (HDP) is superimposed on the PLDOS picture. Hartree potential is the local electrostatic potential of the system governed by Poisson's equation. Far from the interface, the macroscopic average of Hartree potential follows the semiconductor's band bending due to the depletion charge. Close to the interface, the potential is altered by the interface dipole (see **SI.2** available in Supplemental Material at [48]) for more discussions on atomistic modeling of Schottky barrier theory the interface dipole). From **Fig.5.a, i-viii**, as predicted, the depletion region starts to shrink with increased doping. Also, it can be generally observed that the lateral Ag-MoS_2 contacts show a more dominant p-type behavior (smaller p-type barriers compared to n-type barriers). Another interesting feature of PLDOS plots is the visualization of the Metal-Induced Gap States[72] (MIGs). At the location of the physical interface (denoted by yellow dashed lines in **Fig.5a, iv, viii),** DOS in the semiconductor gap does not sharply go to zero. In fact, even a few angstroms away from the actual metallurgical interface, MIGs are present in the midgap and decay into the semiconductor. **Fig.5b** shows the energy distribution of the midgap states on the semiconductor side at the Ag-MoS_2 interface. The presence of MIGs also means there is no clear electronic separation between the semiconductor and the metal in the interface region. Therefore, estimation of barrier height solely through the PLDOS plots will not be accurate since one cannot pinpoint a specific location for the electronic interface.

Extraction of Metal-2D-TMD Barrier Heights

Two methods can be used to extract the barrier height from the DFT-NEGF results. Stradi, *et al*[66] proposed that one can extract the barrier height from the energy difference between the maximum of the $<V_H>$ to the metal's Fermi-level. (see **Figure 5.a, i**). The position of $<V_H>$ maximum indicates the location where the interface dipole begins to affect the potential and serves as a good approximation of the electronic interface position. Unfortunately, this method only works when the polarity of the interface dipole on the semiconductor side has the opposite sign of the depletion charge, which will guarantee the occurrence of an extremum in the Hartree potential. This is the case in the n-type contacts to MoS_2, whereas as the sign of the depletion charge is flipped in p-type contacts, no extrema in $<V_H>$ can be observed anymore (see **SI.1** in Supplemental Material at [48] for more details). Hence, this method cannot be generalized for all contacts.

A more rigorous approach is to extract the barrier heights from the NEGF transport results, which relies on referencing the energy at transmission turn-on with the Schottky barrier height. Transmission spectrum denotes the probability of available states at each energy to transmit through the interface. The minimum energy after which the electrons can conduct is the inherent definition of the electronic barrier height. It can be seen from **Fig.5a, i-viii**, transmission spectrum is always zero in the bandgap since there are no available states to conduct electrons. At energies slightly higher than $E_{C\text{-}NR}$ (Conduction band in the neutral region), when depletion region is present, there are available states on both metal and semiconductor side. However, the barrier at the interface still blocks transmission and *T(E)* stays negligible. It is only at higher energies where electrons gain enough energy to surpass the interface barrier when *T(E)* begins to increase. Interestingly, this onset of transmission turn-on (defined as the point where the *T(E)* reaches 1% of the maximum transmission[73]) coincides well with the maximum of $<V_H>$, which indicates that the first method was successful at predicting the barrier height

At this point, we should emphasize that we intentionally did not use the term "Schottky barrier" when referring to barriers seen in **Fig.5a. i-viii**. First, the barrier heights extracted from the onset of the transmission spectrum are simply activation energies, which are not necessarily equal to the Schottky barrier. For instance, at high doping levels, due to the thinning of the Schottky barrier's width, thermally assisted tunneling current (Thermionic-Field Emission) can conduct through the barrier[19,74](**Fig.5c.ii**). In such cases, the estimated barrier from the transmission spectrum can be smaller than the actual Schottky barrier. Secondly, it is notable that despite the common misconceptions that arise by neglecting the space-charge term in Schottky barrier calculations[19], Schottky barrier itself is inherently dependent on semiconductor's doping and can be substantially lowered (see **Fig.5c.iii**) at doping levels exceeding 10^{20} cm^{-3} [19] (see **SI.1** in Supplemental Material at [48] for doping dependent analysis of the fermi-level pinning). This is also evident **in Figs. 5 a, iv, vii**, wherein due to the presence of near degenerate doping, reduced Schottky barrier and band-bending is observed (no band bending for degenerate case 6.85×10^{14} cm^{-2}). As a consequence of these two effects, at high doping levels, the extracted n-type and p-type Schottky barriers no longer sum to the bandgap of the TMD material. Therefore, the most logical approach to define a canonical Schottky barrier is to report the Schottky barrier at the lowest

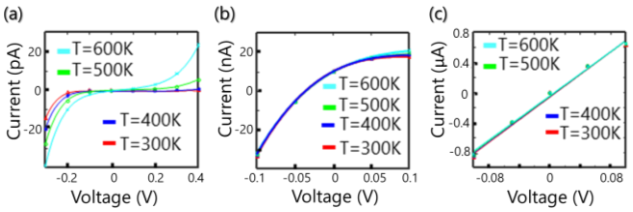

Fig.6. I-V curve at various temperatures (T): (a) at N = 6.85×10^{12} cm^{-2}. Typical thermionic behavior. Note that, due to doping, the onset of reverse bias tunneling current is small. (b) N = 6.85×10^{13} cm^{-2}. I-V curve transitions towards more linear ohmic behavior. (c) N = 6.85×10^{14} cm^{-2}. Fully ohmic behavior. Schottky barrier is transparent to the tunneling current.

feasible doping level, where it is least affected by doping and where transmission spectrum onset corroborates closely with the actual Schottky barrier since thermally assisted tunneling current is negligible (**Fig.5c, ii**). In our calculations, Schottky barriers are reported at 6.85×10^{11} cm^{-2} where the screening length of the depletion region is about ~120Å. It can be observed that at this doping level, the extracted n/p type Schottky barrier sums to approximately 90% of the bandgap **(Fig.5d)**, which shows that doping marginally affects the Schottky barrier and there is no need to probe lower doping levels.

Using the transmission spectrum from NEGF simulations, by integrating over the contributions of available states at each energy level, I-V plot of the interface is calculated through the Landauer formula:

$$\text{Eq.(1)} \quad G = \frac{2q^2}{\hbar}\int T(E)\frac{\partial f}{\partial E}dE$$

where G is the device conductance without bias, q is the elementary charge, ħ is the reduced Planck's constant, *T(E)* is the transmission probability, and f is the Fermi Dirac distribution function. The contact resistance is lastly extracted using the slope of the I-V curve at 0 bias (corresponding to *1/G(0)*) normalized by the cell's width. **Fig.6** shows the calculated I-V curve for three different doping levels at various temperatures. At the lowest doping, all contacts exhibit typical Schottky behavior determined by thermionic emission over the barrier. This can be seen in both rectifying behaviors observed in the I-V characteristics and also from the temperature dependency of the I-V. At intermediate doping, we observed that most contacts transition to Thermionic-Field-Emission, where a swift turn-on of the tunneling current in reverse-bias is observed due to the tunneling through the narrow Schottky barrier. Finally, at degenerate doping, tunneling through the barrier dominates transport and all contacts show complete linear and ohmic characteristics. It is worth mentioning that Fig.6 represents the I-V curve from an asymmetric system of a metal/semiconductor Schottky junction. However, in experiments, a realistic device would be consisting of metal-semiconductor-metal junctions that create two back-to-back Schottky diodes where one junction operates in reverse-bias and the other in forward-bias. Therefore, the actual 2D transistors' response (metal-semiconductor-metal response) at low gate bias (subthreshold) resulting in low electrostatic channel doping would be limited by the Schottky contact's reverse-bias (weaker) branch and exhibits a symmetric behavior w.r.t drain-source voltage.

III. RESULTS

Electrical Properties of Edge

Fig.7a shows the extracted n-type and p-type canonical Schottky barriers for MoS_2 and five different metals at $\pm6.85\times10^{13}$ cm^{-2}. Fitting the Schottky barriers and their associated error bars with the pinned Schottky barrier model (**Fig.3b**), our results suggest that MoS_2 edge contact is pinned to a CNL that lies approximately 665 meV (595-735) meV error margin above the valence band. Given that this margin

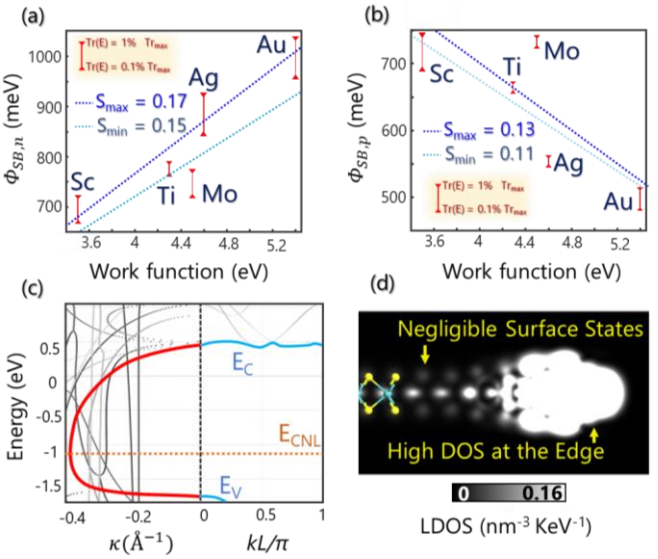

Fig.7. Fermi-level Pinning analysis in Edge-Contacts: (a) n-type Schottky barrier vs metal's work function. **(b)** p-type Schottky barrier vs metal's work function. The error bar for Schottky barriers is extracted by choosing two different thresholds of *T(E)* as the definition for the onset of transmission turn-on. The upper limit is set by the energy at which transmission reaches 1% of maximum transmission and the lower limit is set by energy at which *T(E)* arrives at 0.1% of maximum transmission. **(c)** Complex band structure of 1L-MoS_2 along the in-plane direction. The branching point corresponds to a CNL of 715 meV measured from top of the E_V. **(d)** Local Density of States of terminated Mo-ZZ-2S edge of MoS_2 showing a high density of the terminated states compared to the top interface.

is moderately lower than the mid-gap, this suggests an overall p-type behavior. This contrasts with 2D MoS_2 top contacts where the CNL usually lies closer to the conduction band. Note that the anisotropy between n-type CNL for top contacts and p-type CNL for edge contacts was also predicted by Guo *et al.*[75], which was inferred from the difference between the average energies of orbitals that were relevant to either edge or top conduction. To summarize, the Mo orbitals with symmetry bonding along the cross-plane direction, namely d_{z^2}, $d_{x^2-y^2}$, and d_{xy}, that are responsible for top injection are distributed equally along the valence and conduction bands with energies averaged out to near midgap. Whereas the Mo states with symmetry bonding along the in-plane direction, d_{xz} and d_{yz}, have higher densities in the valence band and result in a CNL closer to the valence band.

The CNL of edge contacts can also be approximated from the branching point of the complex band-structure along the in-plane direction perpendicular to the Mo-ZZ interface. Complex band structure represents the dispersion of the evanescent solutions of Schrodinger's equation which occupy midgap energies when the translational symmetry of the crystal is broken by the interface. In the virtual induced gap states (VIGS) model[76,77], the energy which separates the donor/acceptor-like midgap states is the energy where the penetration length of the evanescent waves reaches its minimum ($E_{k\text{-}max}$) and is called the branching point. In the absence of additional interface state contributors such as

defects and adatoms, branching points will also represent charge neutrality level. From **Fig.7c**, the branching point can be extracted at E_B = ~715 meV, which correlates relatively well with the extracted CNL from the **Fig.7b**.

Furthermore, the pinning factor for both n-type Schottky barrier (S=0.15-0.17) and p-type in edge contacts (S=0.1-0.13) also suggests stronger pinning compared to the theoretical values for pristine top contacts (S=0.3-0.7)[*20,75,78]. This is to be expected as the broken periodicity along the in-plane direction warrants a high density of dangling bonds and evanescent edge-states compared to out-of-plane direction (**Fig.7d**). Also, the marginally stronger pinning factor for p-type Schottky barrier can be attributed to the higher distribution of midgap states toward the valence band **(see Fig.5b).** One should note that the interface states present in our calculations solely originate from the terminated edge states of the semiconductor. There is a possibility that similar to top contacts, additional prevalent defect complexes in edge contacts form and alter this result. Hence, the results are only valid for atomically abrupt edge contacts.

Fig.8.a,b show the extracted contact resistance versus doping of MoS_2 terminated edge with five different metals. As predicted, it is observable that at lower dopings ($N < 10^{13}$ cm^{-2}), the Schottky barrier completely dominates the conduction and metals with lower/higher work functions repeatedly yield better n-type/p-type contacts. Furthermore, at low doping levels ($N < 10^{13}$ cm^{-2}), almost all the metals (except for scandium) show lower p-type contact resistance due to the positioning of the CNL. At intermediate dopings

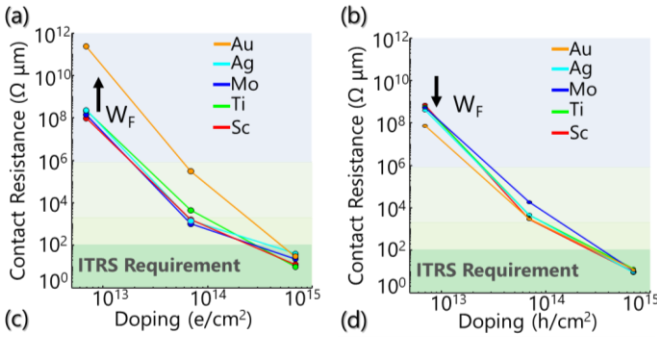

(c)

N-type	6.5*10¹¹ (e/cm²)	6.5*10¹² (e/cm²)	6.5*10¹³ (e/cm²)	6.5*10¹⁴ (e/cm²)
Sc	365 Tr	101 M	1.7 K	13
Ti	523 Tr	226 M	4.6 K	9.6
Mo	585 Tr	146 M	1.09 K	23.9
Ag	14.8 P	1797 M	1.5 K	42.3
Au	1.5e+21	243 G	322 K	31

(d)

P-type	6.5*10¹¹ (e/cm²)	6.5*10¹² (e/cm²)	6.5*10¹³ (e/cm²)	6.5*10¹⁴ (e/cm²)
Sc	224 Tr	633 M	2.86 K	9.79
Ti	156 Tr	490 M	4.3 K	13.14
Mo	259 Tr	458 M	17.5K	10.54
Ag	0.2 Tr	345M	4.48K	9.04
Au	130 G	66 M	2.86K	11.88

Fig.8. Lower limits of edge R_c. (a) Contact resistances for n-type contacts (b) Contact resistances for p-type contacts. The values are extracted at 300K. **(c) Data points for n-type contacts. (d) Data points for p-type contacts.**

[*]Note that the degree of pinning for top contacts (S factor) heavily depends on the fabrication method. For instance, in evaporated or transferred top-contacts almost ideal S-factors, close to 1, have been observed. These results are consistent with DFT simulations in which the Metal preserves a manually fixed large vdW gap. But when in DFT simulations the metal is allowed to geometrically relax on top of the TMD, S factor is not ideal anymore and varies between 0.3-0.7.

$10^{13}<N<10^{14}$ cm^{-2}, contacts transition to Thermionic-Field Emission and contact resistances drop significantly. In a doping region between ~6.85× (10^{13}-10^{14} cm^{-2}), the contacts become completely ohmic, with surprisingly low R_c (<40 Ω μm), well below the ITRS requirements [27]. It is notable that at higher dopings, contacts become less sensitive to the metal work-function, and the dominating factor that determines the contact resistivity becomes the total number of the available modes with matching k-vectors[79] and their transmission probability across the interface. For instance, it is observed that at very high dopings, while both n-type and p-type barriers are negligible, the p-type contact resistances are on average lower than the n-type contacts. Again, this can be ascribed to the higher density of states of in-plane modes in the valence band of MoS_2 as discussed in the last session.

We should emphasize that our ballistic simulation framework does not consider dissipative mechanisms such as electron-phonon, remote phonon, and defect scatterings. Moreover, in practical applications, most doping mechanisms such as substitutional doping will also inevitably introduce detrimental effects such as additional impurity scattering pathways and reduced gate electrostatic control. Therefore, the values reported in this work should be treated as a theoretical upper limit to the electrical performance of the analyzed interfaces. Finally, the high doping concentrations assumed in this work are on par with state-of-the-art CMOS

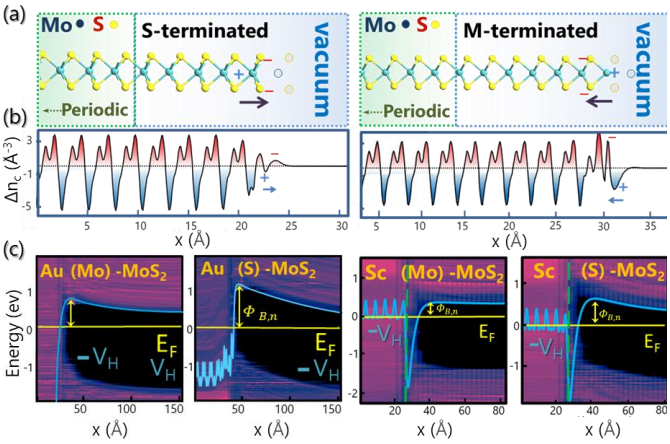

Fig.9. Effect of Sulphur Passivation on Contact Resistance. Due to the polar nature of the Mo-S bonds, two different dipoles form at the edge of different zigzag terminated MoS_2. **(b)** In-plane average of Electron Difference Density (EDD) shows the formation of the dipoles with opposite polarities at the edge. Positive EDD represents electron accumulation and negative, electron depletion. In S-termination, the dipole will increase the effective work-function of the edge, pulling the bands upward while in Mo-termination, dipole reduces the effective edge work-function and pulls the bands downward. **(c) PLDOS of S/Mo terminated MoS_2 with Au and Scandium.** The outcome of different termination edges is best seen by comparing the actual barriers formed in the two different termination cases. Evidently, Mo-termination results in lower n-type Schottky barriers compared to S-terminations. This trend holds true for all the simulated interfaces (Here, Au and Sc are only shown since they represent both ends of the work-function spectrum. See SI.5 for all results in Supplementary Material at [46]).

technologies, which are not yet developed for 2D material platforms. Furthermore, in the immediate future, achieving such doping concentrations solely through the usual gating method would face challenges such as dielectric breakdown and excessive gate-leakage. Therefore, as discussed later in this study, it is essential to study other mitigating solutions to reducing Schottky-barrier.

Revisiting **Fig.7a-b** and **Fig.8**, it seems only Mo contact diverges from the work function trend. Taking a closer look at the contact interface between MoS_2-ZZ edge with sulphur dimers (Mo-ZZ-2S) and Mo, it becomes evident that this interface naturally resembles the interface of a bare MoS_2-ZZ termination with contact metal without the sulphur dimers. This encouraged us to analyze the effect of existence of sulphur passivation in more detail.

Effect of Sulphur Edge-passivation:

To analyze the effect of termination edge in-depth, we carried out our analysis also for MoS_2 with purely Mo terminated zig-zag edges (see **SI.5** in Supplemental Material at [48]). While Mo terminated edges without Sulphur dimers may not be the most thermodynamic stable edge formation of MoS_2, but it is still possible to engineer such interfaces either using in-situ growth [41] or additional annealing steps[80]. We can observe that in contrast to Mo edges with Sulphur passivation, bare Mo terminated edges repeatedly demonstrate lower/higher n-type/p-type Schottky barriers respectively **(Fig.9c)**. Therefore, one can conclude that the charge neutrality level for bare MoS_2 ZZ edges places above the CNL for Sulphur passivated interfaces and is closer to mid-gap and more ambipolar than Sulphur terminated edges. This effect can be attributed to the polarity of the Mo-S bonding, which results in different charge redistribution at the cleaved interface **(Fig.9b).**

Edge Contacts vs Top Contacts:

At this point, we have observed that edge contacts offer lower p-type Schottky barriers compared to top contact geometry. This already suggests that if the transmission rates (normalized w.r.t the top of the Schottky Barrier) for edge contacts are not substantially different than the top contacts, they will have the ability to outperform top contacts in hole conduction. Note that at first sight, one might think that it is not appropriate to compare lateral edge contacts to top contacts as the active atomically-thin interface area for edge contacts is constant and much smaller than what can be achieved in top contacts. This concern is valid. Indeed, if transmission increases as the overlap area increases for top metals, then one cannot compare top contacts to edge contacts on equal footing. In essence, the question returns to whether conduction or injection in top contacts occurs throughout an effective area or happens solely at the edge of the top metal. Prakash *et al*[81] utilized two injection mechanisms to model the 2D metal contacts, path-1, as denoted in **Fig.10a,** presents the path in which the electron is injected from the metal to the 2D channel underneath (Areal Injection) and path-2 is where the electron is injected to the semiconductor at the edge of the metal.

Recent findings[35,36] suggest that as the channel thickness is thinned down, for monolayer 2Ds, conduction via path-1 (under the metal) is heavily suppressed and that the actual,

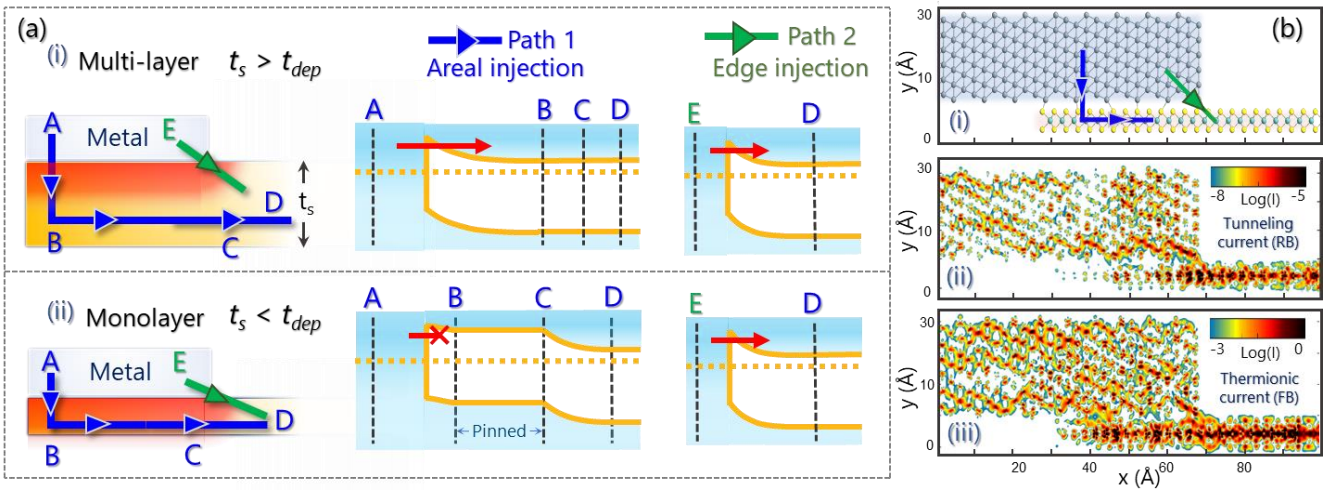

Fig.10. Current injection pathways in monolayer and multi-layer limit. (a) Qualitative band diagrams for injection mechanism in multilayer and monolayer limits: Electron injection can generally be categorized as either injection through the edge of the metal, aka edge injection (green arrow), or injection to the overlapping semiconductor (blue arrow). The red region denotes the depletion region of the semiconductor. (i) When the thickness of the semiconductor is larger than the depletion length, there is no difference between barrier from path-1 and path-2. (ii) For very thin semiconductors such as monolayer MoS_2, the Schottky barrier is barely screened in the vertical direction (A to B). Fermi-level of the semiconductor under the metal is pinned to a level determined by the top metal (region B-C) and the semiconductor under metal can be considered fully depleted. In this case, the electron cannot tunnel to the overlap region since there are no available states and effectively the areal current will be suppressed. However, path-2's barrier remains untouched. **(b) Current Density**. Current density plots for Au-MoS_2 (1L) top contacts with $N = 6.85 \times 10^{12}$ cm^{-2}. (i) atomic configuration of the interface (ii) Current density plot at the onset of transmission turn-on for the reverse-biased junction (V_{RB} = 0.3 V). Tunneling current occurs through path-1 and is suppressed under the metal. (iii) Current density plot at the onset of transmission turn-on for a forward-biased junction (V_{FB} = 0.1 V). Thermionic current flows through both path-1 and path-2.

effective injection occurs solely at the edge of the metal (path two). Our findings corroborate these results. This is best understood by comparing the qualitative band profiles of different injection mechanisms in monolayer and multilayer TMDs. For multilayer TMDs, the depletion region along path-1 has sufficient space to screen in the vertical direction (see A-B in **Fig.10a-i**). Therefore, in the reverse-bias region, the electrons using thermally assisted tunneling can conduct through the Schottky barrier to the semiconductor under the metal and flow laterally to the electrode. However, in the monolayer limit, the Schottky barrier is barely screened in the vertical direction (see A-B in **Fig.10a-ii**) and the Fermi-level inside the semiconductor is pinned to a level determined by the top metal's Fermi-level pinning[78]. In this case, electrons can no longer tunnel to the metal underneath since there are no available states in the semiconductor at the same energy. Hence, in the monolayer limit, the conduction via path-1 is suppressed, but the conduction through path-2 remains the same for both monolayer and multilayer semiconductors (see edge injection band alignment in **Fig.10a**), and the total current becomes dominated by edge-injection (path-2) for monolayer. Note that the ratio of the contribution between path-2 and path-1 will depend on the V_{DS}, Fermi-level pinning position of the top contact, and the type of the gate.

One should also note that this analysis is only valid when the contact is reverse-biased. If contact is in the forward-bias region, the total current through the device is dominated by thermionic emission, which implies that there will be no difference between path-1 and path-2. This can be seen in **Fig. 10b, ii-iii**, where we present current density across the top contact device. Given that reverse-bias junction is the limiting factor to contact resistance of the total device, we can

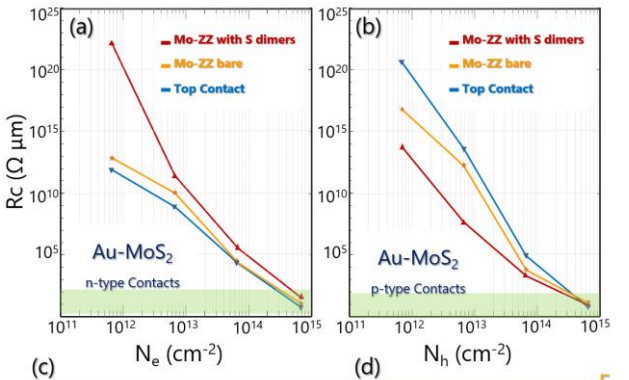

Contact type	Φ_n(meV)	Φ_p (meV)
Top contact	461	996
Mo-ZZ Edge with S dimers	953	490
Mo-ZZ- Edge bare	632	716

Fig.11. Performance of Au-MoS_2 edge contacts vs top contacts. **(a)** Electron injection, R_c vs electron density **(b)** Hole injection, R_c vs hole density. **(c)** Comparison of measured Schottky barriers. **(d)** A qualitative sketch illustrating the Fermi-level pinning in different contact geometries.

conclude that for monolayer TMDs, it is fair to compare edge and top contacts, as in both, effective injections occur across the edge of the metal.

To test this hypothesis and compare the edge contacts to pristine top contacts, we simulated top/edge contact formations between MoS_2 and Au using the same framework presented earlier (see **SI.6** for simulation details in Supplemental Material at [48]). As expected, the top-contact between Au-MoS_2 yields smaller/larger n-type/p-type barrier w.r.t edge contacts due to the difference in the CNL of top interfaces **(Fig.11c).** Extracted contact resistances **(Fig.11a-b)** demonstrate that, at the same doping level, the edge contacts can surpass top contacts by over an order of magnitude due to the lower Schottky barrier. However, edge contacts cannot outperform top contacts in electron conduction. These results suggest that any enhancement in transmission rates in edge contacts that might occur due to the elimination of the vdW barrier has a marginal effect on contact resistance. In fact, the charge redistribution caused by strong covalent bonding at the edge interface more strongly pins the Fermi-level to energies below midgap **(Fig.11d),** which hinders the n-type electron transport. It is readily observable that the effect of this pinning far exceeds any improvement to contact resistance due to the elimination of the vdW gap.

Schottky Barrier Inhomogeneity, Hybrid Contacts, and the Effect of Imperfect Edge Formations:

At the first glance, the inhomogeneity between the Fermi-level pinning at edge and top interface appears to be an excellent opportunity to achieve both n-type and p-type low contact resistances by simultaneously contacting both the edge and top interfaces in a "hybrid contact" scheme as illustrated in **Fig.12a**. Here we argue that such hybrid contacts may only be advantageous in contacts to multilayer TMDs. Note that the formation of such hybrid contacts, with a metal overlap on the top TMD surface, is also highly likely to happen unintentionally during the fabrication of edge contacts using the *h*-BN encapsulation technique. This is because to expose the TMD edge, the *h*-BN/TMD stack must be etched at an angle that will inadvertently expose some of the TMD surfaces as well (imperfect edge-contacts).

To comprehend the effect of the overlapping metal in hybrid contacts, we further studied the interface of Au-monolayer-MoS_2 hybrid contacts **(Fig.12a)** using the established framework (see **SI.7** for details in Supplemental Material at [48]). **Fig.12c** shows the overall band alignment of a hybrid contact between Au-MoS_2 (p-type configuration). It is observed that the Schottky barrier at the edge still retains its dominant p-type behavior. However, holes still cannot enter the semiconductor at the lower Schottky barrier in the edge (represented by blue arrows) since the potential inside the semiconductor immediately after the edge is pinned to a lower value by the Fermi-level pinning effect of the top metal. This increases the effective p-type barrier that is determined by the top-metal. Note that this effect is again caused by the marginal screening of the semiconductor's

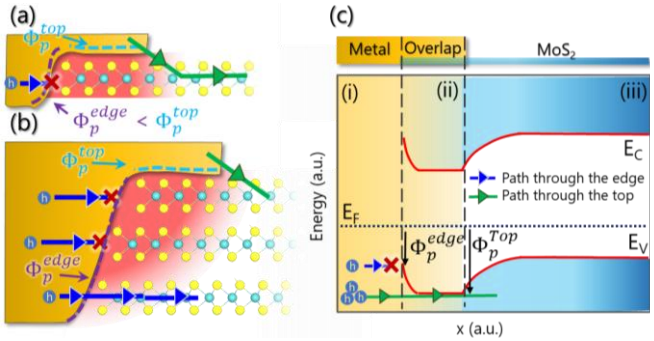

Fig.12. Hybrid contacts and exploiting Schottky barrier inhomogeneity: (a) Schematic representation of a hybrid contact to monolayer MoS_2. The red area denotes the depletion region. Purple dashes represent the low hole barrier caused by Fermi-level pinning at the edge region. Cyan blue dashes represents the high hole barrier/low electron barrier caused by Fermi-level pinning at the top-surface. The depletion region created by the Fermi-level pinning from the top surface of the contact prohibits conduction of holes from the smaller p-type barrier at the edge, raising the effective hole barrier from the edge to the same value as the top surface. **(b)** Schematic representation of hybrid contacts to multilayer MoS_2. The screening of the depletion region now allows the holes to conduct through the lower p-type barrier of the edge at the lower layers. **(c)** Schematic band-alignment of a hybrid contact to monolayer MoS_2. Note that the Fermi-level in the semiconductor under contact is governed by the Fermi-level pinning of top-contact. In the meantime, TMD edge still retains its low p-type Schottky barrier, however, the effective barrier for holes at the edge (blue arrow) is increased by the n-type pinning of the top-contact.

potential in the vertical direction (depletion region due to top contact depicted as the red region) similar to edge-injection effects in **Fig.10a-ii**. As the number of layers increases and the depletion width is screened in the vertical direction under the metal **(Fig.12b)**, top-metal no longer affects the barrier for holes in the edge-interfaces of bottom MoS_2 layers and therefore, holes can now conduct at lower Schottky barrier energies for the edge. Therefore, these types of hybrid contacts (or imperfect edge contacts) will have a dominant n-type behavior at the monolayer limit (as the Schottky barrier is dominated the by lower n-type Schottky barrier for top contacts) and as the thickness of the 2D flake is increased, the contact becomes dominantly p-type. This trend was also observed in recent experimental studies[40,43], while there it was attributed to weak-Fermi level pinning at the edge, here we argue it is, in fact, a consequence of inhomogeneous Schottky barriers at the edge and top interfaces. Overall, our results demonstrate that, in the monolayer limit, to leverage the low p-type Schottky barrier at the edge contact, the junction must become as abrupt as possible with minimum overlap area. Another way to circumvent this limitation and to leverage the Schottky barrier inhomogeneity for n-type and p-type conduction is to use multi-layer (3D) source/drain regions while maintaining the channel atomically thin. We will describe this approach more in-depth in the outlook section.

MoS_2-Graphene Lateral Contact and Dynamic Reduction of Schottky barrier:

Our analysis up until this point has been primarily focused on interfaces of conventional bulk (3D) materials with 2D MoS_2. However, a research opportunity has been made available in the realm of 2D-graphene lateral heterojunction. This approach is inspired by the concept of seamless/edge contacted all-2D circuits[33,82]. 2D-graphene lateral contacts offer a unique advantage over traditional 3D-2D edge contacts in that their Schottky barrier can be modulated via the gate electrostatics, an effect we call dynamic control of the Schottky barrier. Graphene is a semi-metal with low DOS near the Dirac point (low-quantum capacitance). Therefore, upon application of an electric field, to accommodate for the accumulated charge, the Fermi-level in graphene moves to higher/lower energies (depending on the gate polarity) which effectively changes graphene's work-function **(Fig.13a).** This effect can be leveraged in the device designs where the gate overlaps the graphene-TMD interface **(Fig.13b)** to allow for a dynamic reduction in the Schottky barrier as the device is turned on[83]. To simulate this effect, we used an in-house NEGF code[4] based on tight-binding model to solve the NEGF and Poisson's equation iteratively to obtain the potential distribution, local density of states, and the carrier density for Graphene-MoS_2-Graphene lateral heterostructure (See **SI.8** for more details in Supplemental Material at [48]). In the simulation domain, the gate not only covers the channel but also overlaps the graphene interface to mimic the electrostatic gating. **Fig.13c** represents the simulated LDOS and band-diagram of a graphene-MoS_2-graphene device with applied gate voltage. It is readily observable that due to low DOS of graphene, Dirac point in graphene is pulled down close to the interface, leading to a smaller n-type Schottky barrier w.r.t the off state. The high conductivity graphene, which also helps reduce the series resistance of the Graphene-WS_2-Graphene heterostructure in field-effect transistors applications, along with dynamically tunable Schottky barrier has shown record-breaking ON-current with contact resistances as low as 0.67 kΩ μm[83].

The synthesis of Graphene-TMD lateral heterostructures is usually done by carving out a window in graphene proceeded by the growth of TMD from the graphene's edge nucleation sites using CVD or MOCVD techniques. Interestingly, the morphology of the graphene-TMD interface is not an abrupt atomic junction but, as repeatedly demonstrated[83–86], an effective overlap area is created on top of the graphene by the TMD. This overlap can be as small as 2 nm based on growth conditions. Hence, technically the synthesized Graphene-TMD lateral heterostructures are not pure edge-contacts and more in-line with a hybrid or top-contact configuration.

The degree of the performance boost from the work-function modulation is directly proportional to the pinning factor of the graphene-TMD interface (at intermediate doping levels where the contact is determined by thermionic or thermally assisted field emission). For instance, at a true Schottky-Mott limit (S=1) the Schottky barrier modulation effect should theoretically yield high-performance ambipolar transistors.

However, due to the presence of intrinsic defects in TMD, the Fermi-level pinning is inevitable in most experimental demonstration and fabricated devices demonstrate a strong mode-mismatch. However, recently, Cao *et al*[87]. leveraging the band-alignment between graphene and WSe_2, have been able to demonstrate a balanced gate tunable ambipolar TMD transistor without mode mismatch.

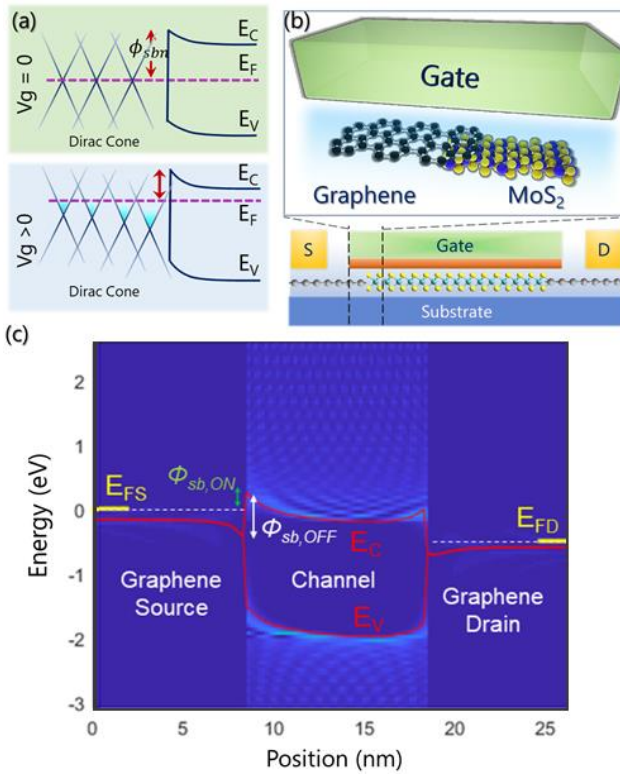

Fig.13. Dynamic reduction of Schottky barrier: (a) Qualitative band-alignment of Graphene-MoS_2 Schottky barrier. **(b)** Gated graphene-MoS_2 interface in a lateral graphene-MoS_2 FET **(c)** LDOS plot of the Graphene-MoS_2-Graphene heterostructure with applied gate. As the gate turns on, Fermi-level in graphene moves to higher energies and its work-function is lowered, which results in a reduction of Schottky barrier height.

Overall, graphene-TMD heterostructures with their potential in large-scale manufacturability[83,88], high interfacial thermal conductivities[89], and dynamically tunable Schottky barrier show a promising path toward the realization of high-performance devices in the near future.

IV. Outlook

It should be emphasized that the interfaces under study are purely defect-free interfaces. Similar to the presence of defect complexes in 2D top contacts, which govern the electrical conduction through the top, electrical properties of edge contacts can also be susceptible to inevitable defect formations at the edge. Further ab-initio simulations and experimental characterizations are required to identify probable defect complexes that may occur in different edge contact fabrication techniques. Furthermore, the strong Fermi-level pinning caused by covalent bonding in the pristine edge contacts will hinder their contact resistance in the near future since no reliable doping technology has yet been developed for 2D TMDs. In the meantime, it might be advantageous to explore other unorthodox solutions. For instance, demonstration of selective area intercalation [90] can be a promising pathway to degenerately dope the area adjacent to metal contacts. Moreover, edge-contacts do not necessarily have to form between pristine 2H phase TMDs and contacting metals. Phase engineering methods, such as converting 2H phase MoS_2 to 1T phase in the immediate contact region[91], have shown promise in improving contact properties. Such phase engineering methods can also be utilized for edge contacts as an alternative to degenerate doping provided the metallic phase can be made stable. Approaches such as roughness engineering can be used to increase the edge-length/contact area ratio to achieve lower contact resistance[20]. Meanwhile, graphene/TMD edge-contacts have shown the best overall performance as attributed to their unique contact gating properties[83].

As mentioned earlier, the range of achieved contact resistances in demonstrations of edge contacts varies by over 4 orders with a few seemingly contradictory results. For instance, Choi[40] and Moon[39] have reported dominant n-type behavior in Au-MoS_2 edge contacts whereas Yang[43] has reported a strong p-type behavior in Au-MoS_2 edge contacts. Intriguingly, both n-type Schottky barriers of less than 50 meV and p-type negative Schottky barriers have been reported in Au-MoS_2, even though the contact resistances are in the MΩ μm range. This apparent contradiction between measured Schottky barriers and contact resistances have been attributed to the atomically narrow one-dimensional active cross-section of the MoS_2 edge, however as shown in this work and other experimental papers[91], contact resistances as low as 200 Ω μm have been achieved solely through edge contacts to MoS_2, therefore the limited active cross-section in itself cannot be the sole reason. Yang[43] has argued that edge contacts perform close to Schottky-Mott limit (S=1), however, results from Cheng, Yang, and Moon, in which Au-MoS_2 and Ni-MoS_2 contacts (Au and Ni's work-functions are 5.4 eV and 5.2 eV respectively, which should yield strong p-type contacts) show a dominant n-type branch that is not in line with their observation. It is evident at this point that the specific interface atomic configuration of different edge contact demonstrations varies from method to method. While our analysis of imperfect edge contacts in this manuscript can justify some of these apparent contradictions, such as n-type to p-type dominant transition of Au-MoS_2 edge contacts with increased thickness of TMD flake, further experimental TEM/STEM characterizations are needed to shed light on the atomic morphology of the edge interfaces achieved via different fabrication methods. Formation of de-pinning oxide layers and strain-induced 1T' phases[92] is also probable and can justify some of these experimental observations. Furthermore, care must be taken when applying the flat-band

Schottky barrier extraction method[58] to 1D contacts. It should be emphasized that estimating the Schottky barrier from the flat-band condition is only viable when the gate has not reached the threshold voltage, which can lead to a misconstruction of negative Schottky barriers[21]. Finally, during the analysis of the Schottky barrier when using the flat-band method, the exact power of the temperature term relative to the number of layers exists in a gray area, which can introduce uncertainties to the extracted results. In the future, electro-optical Schottky barrier measurement techniques must be employed to circumvent these problems and optimize the all electrical flat-band measurement methods to yield more accurate estimations.

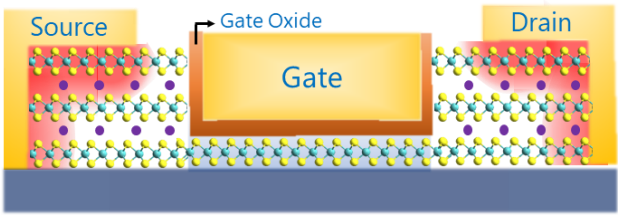

Fig.14. Proposed 2D FET with raised intercalated source/drain. Purple dot denotes the foreign intercalant agents which dope the source-drain region. The red shades denote the boundary of the Schottky barrier width. The 3D nature of the source-drain maximizes the available electron injection pathways compared to the limited narrow injection path in regular 1L 2D FETs. Moreover, this design can leverage the Schottky barrier inhomogeneity of top and edge interfaces to achieve complimentary operation.

Finally, it is important to emphasize that the suppression of areal injection current mechanism (**Fig.10b**) in contacts to monolayer TMDs indicates that these contacts are much more susceptible to current crowding effects. It is still unclear to what extent such current crowding effects, which can impact the device self-heating and performance, and thereby chip-scale power dissipation and reliability of nanoscale ICs[93], complicate the future 2D transistor architectures. Further studies are required to ascertain how the semiconductor doping is able to relieve the potential current crowding effects. However, a design consideration can be derived to alleviate this problem, which is to use 3D (multi-layer) source/drain region while keeping the channel monolayer (**Fig.14**), to allow sufficient space for the screening of the Schottky barrier potentials near the source-drain electrodes. This design in effect allows for areal current injection pathways, which can relieve the contact resistance during potential current crowding scenarios. An interesting addendum to this design is that the multi-layer source-drain regions are suitable for intercalation doping[94–96] whereas the monolayer channel, due to its thickness, can be expected to remain unaffected by intercalation processes. Several technological problems must be addressed to make this type of design feasible. First, etching the channel down to a monolayer is a challenging task using conventional etchants. Atomic layer etching techniques on 2D TMDs must be perfected to achieve this capability. Furthermore, the reliability and stability of the selective area intercalation process must be studied in order to assess their manufacturability.

V. Conclusion

In summary, our results show that 1D edge contacts to 2D monolayer MoS_2 are typically dominated by a p-type conduction mechanism due to the placement of their charge neutrality level close to the valance band. Moreover, we can observe bare Mo-ZZ terminated edge contacts can achieve better n-type contacts compared to the sulphur passivated Mo-terminated contacts. At high doping levels, 1D contacts can supersede top contact in p-type conduction and achieve lower contact resistances, despite their atomically thin overlap. Furthermore, we reveal that as a consequence of the Schottky barrier inhomogeneity between the top and edge interfaces, it is essential to achieve abrupt 2D-2D lateral junctions without any metal overlap in order to utilize the lower p-type Schottky barrier in edge contacts. Nevertheless, from a practical perspective, the dynamic tunability of the SB at the Gr-TMD lateral heterojunctions that leverages some overlap between the Gr and TMD provides an interesting case in study. Likewise, FETs with 3D raised source/drain geometries are preferred which can leverage this Schottky-barrier inhomogeneity while maximizing the available current injection pathways, thereby enabling 2D-FETs to achieve their true predicted potential.

Acknowledgment

This research was supported by the ARO (grant W911NF1810366) and the Japan Science and Technology Agency (JST) Core Research for Evolutional Science and Technology (CREST) Program under Grant SB180064. Use was made of computational facilities purchased with funds from the National Science Foundation (CNS-1725797) and administered by the Center for Scientific Computing (CSC). The CSC is supported by the California NanoSystems Institute and the Materials Research Science and Engineering Center (MRSEC; NSF DMR 1720256) at UC Santa Barbara.

References

[1] K. S. Novoselov *et al.*, “Two-dimensional atomic crystals,” *Proc. Nat. Acad. Sci.* USA, vol. 102, no. 30, pp. 10451–10453, 2005.

[2] B. Radisavljevic, A. Radenovic, J. Brivio, V. Giacometti, and A. Kis, “Single-layer MoS2 transistors,” *Nat. Nanotechnol.*, vol. 6, no. 3, pp. 147–150, 2011, doi: 10.1038/nnano.2010.279.

[3] Y. Yoon, K. Ganapathi, and S. Salahuddin, “How good can monolayer MoS2 transistors be?,” *Nano Lett.*, vol. 11, no. 9, pp. 3768–3773, 2011, doi: 10.1021/nl2018178.

[4] W. Cao, J. Kang, D. Sarkar, W. Liu, and K. Banerjee, “2D Semiconductor FETs - Projections and design for Sub-10 nm VLSI,” *IEEE Trans. Electron Devices*, vol. 62, no. 11, pp. 3459–3469, 2015, doi: 10.1109/TED.2015.2443039.

[5] S. Kim et al., “High-mobility and low-power thin-film transistors based on multilayer MoS_2 crystals,” *Nat. Commun.*, vol. 3, pp. 1011–1017, 2012, doi: 10.1038/ncomms2018.

[6] J. Jiang, K. Parto, W. Cao, and K. Banerjee, “Ultimate monolithic-3D Iintegration with 2D materials: rationale, prospects, and challenges,” *IEEE J. Electron Devices Soc.*, vol. 7, pp. 878–887, 2019, doi: 10.1109/jeds.2019.2925150.

[7] D. Xiao, G. Bin Liu, W. Feng, X. Xu, and W. Yao, “Coupled spin

and valley physics in monolayers of MoS_2 and other group-VI dichalcogenides," *Phys. Rev. Lett.*, vol. 108, no. 19, pp. 1–5, 2012, doi: 10.1103/PhysRevLett.108.196802.

[8] K. F. Mak, K. He, J. Shan, and T. F. Heinz, "Control of valley polarization in monolayer MoS_2 by optical helicity," *Nat. Nanotechnol.*, vol. 7, no. 8, pp. 494–498, 2012, doi: 10.1038/nnano.2012.96.

[9] K. F. Mak, K. L. McGill, J. Park, and P. L. McEuen, "The valley hall effect in MoS_2 transistors," *Science*, vol. 344, no. 6191, pp. 1489–1492, 2014, doi: 10.1126/science.1250140.

[10] J. R. Schaibley *et al.*, "Valleytronics in 2D materials," *Nat. Rev. Mater.*, vol. 1, no. 11, 2016, doi: 10.1038/natrevmats.2016.55.

[11] K. He, C. Poole, K. F. Mak, and J. Shan, "Experimental demonstration of continuous electronic structure tuning via strain in atomically thin MoS_2, " *Nano Lett.*, vol. 13, no. 6, pp. 2931–2936, 2013, doi: 10.1021/nl4013166.

[12] P. Rivera *et al.*, "Observation of long-lived interlayer excitons in monolayer MoSe 2-WSe 2 heterostructures," *Nat. Commun.*, vol. 6, pp. 4–9, 2015, doi: 10.1038/ncomms7242.

[13] K. Tran *et al.*, "Evidence for moiré excitons in van der Waals heterostructures," *Nature*, vol. 567, no. 7746, pp. 71–75, 2019, doi: 10.1038/s41586-019-0975-z.

[14] Y. M. He *et al.*, "Single quantum emitters in monolayer semiconductors," *Nat. Nanotechnol.*, vol. 10, no. 6, pp. 497–502, 2015, doi: 10.1038/nnano.2015.75.

[15] M. Toth and I. Aharonovich, "Single photon sources in atomically thin materials," *Annu. Rev. Phys. Chem.*, vol. 70, no. 1, pp. 123–142, 2019, doi: 10.1146/annurev-physchem-042018-052628.

[16] D. Chimene, D. L. Alge, and A. K. Gaharwar, "Two-Dimensional nanomaterials for biomedical applications: Emerging trends and future prospects," *Adv. Mater.*, vol. 27, no. 45, pp. 7261–7284, 2015, doi: 10.1002/adma.201502422.

[17] D. Sarkar, W. Liu, X. Xie, A. C. Anselmo, S. Mitragotri, and K. Banerjee, "MoS_2 field-effect transistor for next-generation label-free biosensors," *ACS Nano*, vol. 8, no. 4, pp. 3992–4003, 2014, doi: 10.1021/nn5009148.

[18] P. Ajayan, P. Kim, and K. Banerjee, "Two-dimensional van der Waals materials," *Phys. Today*, vol. 69, no. 9, pp. 38–44, 2016, doi: 10.1063/PT.3.3297.

[19] S. M. Sze and K. K. Ng, *Physics of Semiconductor Devices: Third Edition*. 2006.

[20] J. Kang, W. Liu, D. Sarkar, D. Jena, and K. Banerjee, "Computational study of metal contacts to monolayer transition-metal dichalcogenide semiconductors," *Phys. Rev. X*, vol. 4, no. 3, pp. 1–14, 2014, doi: 10.1103/PhysRevX.4.031005.

[21] A. Allain, J. Kang, K. Banerjee, and A. Kis, "Electrical contacts to two-dimensional semiconductors," *Nat. Mater.*, vol. 14, no. 12, pp. 1195–1205, 2015, doi: 10.1038/nmat4452.

[22] W. Liu, J. Kang, D. Sarkar, Y. Khatami, D. Jena, and K. Banerjee, "Role of metal contacts in designing high-performance monolayer n-type WSe2 field effect transistors," *Nano Lett.*, vol. 13, no. 5, pp. 1983–1990, 2013, doi: 10.1021/nl304777e.

[23] D. S. Schulman, A. J. Arnold, and S. Das, "Contact engineering for 2D materials and devices," *Chem. Soc. Rev.*, vol. 47, no. 9, pp. 3037–3058, 2018, doi: 10.1039/c7cs00828g.

[24] J. Kang, W. Liu, and K. Banerjee, "High-performance MoS_2 transistors with low-resistance molybdenum contacts," *Appl. Phys. Lett.*, vol. 104, no. 9, pp. 2–7, 2014, doi: 10.1063/1.4866340.

[25] M. Gurram, S. Omar, and B. J. V. Wees, "Bias induced up to 100% spin-injection and detection polarizations in ferromagnet/bilayer-hBN/graphene/hBN heterostructures," *Nat. Commun.*, vol. 8, no. 1, pp. 1–7, 2017, doi: 10.1038/s41467-017-00317-w.

[26] A. Pal, K. Parto, K. Agashiwala, W. Cao, and K. Banerjee, "Computational study of spin injection in 2D Materials," in *IEDM Tech. Dig.*, Dec. 2019, pp. 578–581, 2019.

[27] 2015 International Technology Roadmap for Semiconductors (ITRS). Available: http://www.itrs2.net/

[28] Y. Taur and T. H. Ning, *Fundamentals of Modern VLSI Devices*. Cambridge University Press, 2009.

[29] P. Luo *et al.*, "Doping engineering and functionalization of two-dimensional metal chalcogenides," *Nanoscale Horizons*, vol. 4, no. 1, pp. 26–51, 2019, doi: 10.1039/c8nh00150b.

[30] Y. Khatami, H. Li, C. Xu, and K. Banerjee, "Metal-to-multilayer-graphene contact part I: Contact resistance modeling," *IEEE Trans. Electron Devices*, vol. 59, no. 9, pp. 2444–2452, 2012, doi: 10.1109/TED.2012.2205256.

[31] Y. Wang *et al.*, "Van der Waals contacts between three-dimensional metals and two-dimensional semiconductors," *Nature*, vol. 568, no. 7750, pp. 70–74, 2019, doi: 10.1038/s41586-019-1052-3.

[32] J. Kang, J *et al.*,. "A computational study of metal-contacts to beyond-graphene 2D semiconductor materials," in in *IEDM Tech. Dig.* 2012, pp 407–410, doi:10.1109/IEDM.2012.6479060.

[33] J. Kang, D. Sarkar, Y. Khatami & K. Banerjee, "Proposal for all-graphene monolithic logic circuits," *Appl. Phys. Lett.*, vol. 103, pp. 1–6, 2013, doi: 10.1063/1.4818462.

[34] W. Cao, M. Huang, C. H. Yeh, K. Parto, and K. Banerjee, "Impact of transport anisotropy on the performance of van der Waals materials-based electron devices," *IEEE Trans. Electron Devices*, vol. 67, no. 3, pp. 1310–1316, 2020, doi: 10.1109/TED.2020.2970394.

[35] G. Arutchelvan *et al.*, "From the metal to the channel: A study of carrier injection through the metal/2D MoS_2 interface," *Nanoscale*, vol. 9, no. 30, pp. 10869–10879, 2017, doi: 10.1039/c7nr02487h.

[36] Á. Szabó, A. Jain, M. Parzefall, L. Novotny, and M. Luisier, "Electron transport through Metal/MoS_2 interfaces: Edge- or area-dependent process?," *Nano Lett.*, vol. 19, no. 6, pp. 3641–3647, 2019, doi: 10.1021/acs.nanolett.9b00678.

[37] Z. Cheng *et al.*, "Immunity to contact scaling in MoS_2 transistors using in situ edge contacts," *Nano Lett.*, vol. 19, no. 8, pp. 5077–5085, 2019, doi: 10.1021/acs.nanolett.9b01355.

[38] Y. Chai, R. Ionescu, S. Su, R. Lake, M. Ozkan, and C. S. Ozkan, "Making one-dimensional electrical contacts to molybdenum disulfide-based heterostructures through plasma etching," *Phys. Status Solidi Appl. Mater. Sci.*, vol. 213, no. 5, pp. 1358–1364, 2016, doi: 10.1002/pssa.201532799.

[39] B. H. Moon *et al.*, "Junction-structure-dependent Schottky barrier inhomogeneity and device ideality of monolayer MoS_2 field-effect transistors," *ACS Appl. Mater. Interfaces*, vol. 9, no. 12, pp. 11240–11246, 2017, doi: 10.1021/acsami.6b16692.

[40] H. Choi *et al.*, "Edge contact for carrier injection and transport in MoS_2 field-effect transistors," *ACS Nano*, vol. 13, no. 11, pp. 13169–13175, Nov. 2019, doi:10.1021/acsnano.9b05965.

[41] C. H. Chu, H. C. Lin, C. H. Yeh, Z. Y. Liang, M. Y. Chou, and P. W. Chiu, "End-bonded metal contacts on WSe_2 field-effect transistors," *ACS Nano*, vol. 13, no. 7, pp. 8146–8154, 2019, doi: 10.1021/acsnano.9b03250.

[42] A. Jain *et al.*, "One-dimensional edge contacts to a monolayer semiconductor," *Nano Lett.*, vol. 19, no. 10, pp. 6914–6923, 2019, doi: 10.1021/acs.nanolett.9b02166.

[43] Z. Yang *et al.*, "A Fermi-level-pinning-free 1D electrical contact at the intrinsic 2D MoS_2–Metal junction," *Adv. Mater.*, vol. 31, no. 25, pp. 1–9, 2019, doi: 10.1002/adma.201808231.

[44] C. C. Cheng *et al.*, "First demonstration of 40-nm channel length top-gate WS2 pFET using channel area-selective CVD growth directly on SiOx/Si substrate," *Dig. Tech. Pap. - Symp. VLSI Technol.*, vol. 2019-June, pp. T244–T245, 2019, doi: 10.23919/VLSIT.2019.8776498.

[45] L. Wang *et al.*, "One-dimensional electrical contact to a two-dimensional material," *Science*, vol. 342, no. 6158, pp. 614–617, 2013, doi: 10.1126/science.1244358.

[46] See Supporting Material at [insert link please]

[47] C. Mead, W. Spitzer, and F. L. Position, "Fermi level position at metal-semiconductor interfaces," *Phys. Rev.*, vol. 134, no. 3A, pp. A713–A716, 1964, doi: 10.1103/PhysRev.134.A713.

[48] J. Tersoff, "Schottky barrier heights and the continuum of gap states," *Phys. Rev. Lett.*, vol. 52, no. 6, pp. 465–468, 1984, doi: 10.1103/PhysRevLett.52.465.

[49] R. T. Tung, "Formation of an electric dipole at metal-semiconductor interfaces," *Phys. Rev. B - Condens. Matter Mater. Phys.*, vol. 64, no. 20, pp. 1–15, 2001, doi: 10.1103/PhysRevB.64.205310.

[50] R. T. Tung, "The physics and chemistry of the Schottky barrier height," *Appl. Phys. Rev.*, vol. 1, no. 1, 2014, doi: 10.1063/1.4858400.

[51] Y. Y. Illarionov et al., "Insulators for 2D nanoelectronics: the gap to bridge," *Nat. Commun.*, vol. 11, no. 1, 2020, doi: 10.1038/s41467-020-16640-8.

[52] D. Liu, Y. Guo, L. Fang, and J. Robertson, "Sulfur vacancies in monolayer MoS_2 and its electrical contacts," *Appl. Phys. Lett.*, vol. 103, no. 18, 2013, doi: 10.1063/1.4824893.

[53] S. McDonnell, R. Addou, C. Buie, R. M. Wallace, and C. L. Hinkle, "Defect-dominated doping and contact resistance in MoS_2," *ACS Nano*, vol. 8, no. 3, pp. 2880–2888, 2014, doi: 10.1021/nn500044q.

[54] Y. Guo, D. Liu, and J. Robertson, "Chalcogen vacancies in monolayer transition metal dichalcogenides and Fermi level pinning at contacts," *Appl. Phys. Lett.*, vol. 106, no. 17, 2015, doi: 10.1063/1.4919524.

[55] R. Addou, L. Colombo, and R. M. Wallace, "Surface defects on Natural MoS_2," *ACS Appl. Mater. Interfaces*, vol. 7, no. 22, pp. 11921–11929, 2015, doi: 10.1021/acsami.5b01778.

[56] P. Bampoulis, R. Van Bremen, Q. Yao, B. Poelsema, H. J. W. Zandvliet, and K. Sotthewes, "Defect dominated charge transport and Fermi Level Pinning in MoS_2/Metal contacts," *ACS Appl. Mater. Interfaces*, vol. 9, no. 22, pp. 19278–19286, 2017, doi: 10.1021/acsami.7b02739.

[57] R. T. Tung, "Recent advances in Schottky barrier concepts," *Mater. Sci. Eng. R Reports*, vol. 35, no. 1–3, pp. 1–138, 2001, doi: 10.1016/S0927-796X(01)00037-7.

[58] S. Das, H. Y. Chen, A. V. Penumatcha, and J. Appenzeller, "High performance multilayer MoS_2 transistors with scandium contacts," *Nano Lett.*, vol. 13, no. 1, pp. 100–105, 2013, doi: 10.1021/nl303583v.

[59] C. Maurel, F. Ajustron, R. Péchou, G. Seine, and R. Coratger, "Electrical behavior of the Au/MoS_2 interface studied by light emission induced by scanning tunneling microscopy," *Surf. Sci.*, vol. 600, no. 2, pp. 442–447, 2006, doi: 10.1016/j.susc.2005.10.042.

[60] M. Abraham and S. E. Mohney, "Annealed Ag contacts to MoS_2 field-effect transistors," *J. Appl. Phys.*, vol. 122, no. 11, 2017, doi: 10.1063/1.4991961.

[61] E. Gourmelon, J. C. Bernède, J. Pouzet, and S. Marsillac, "Textured MoS_2 thin films obtained on tungsten: Electrical properties of the W/MoS2 contact," *J. Appl. Phys.*, vol. 87, no. 3, pp. 1182–1186, 2000, doi: 10.1063/1.372061.

[62] C. Kim *et al.*, "Fermi level pinning at electrical metal contacts of monolayer molybdenum dichalcogenides," *ACS Nano*, vol. 11, no. 2, pp. 1588–1596, 2017, doi: 10.1021/acsnano.6b07159.

[63] Synopsys QuantumATK. Version O-2019.03. [Online]. Available: https:// www.synopsys.com/silicon/quantumatk.htm

[64] S. Smidstrup *et al.*, "QuantumATK: An integrated platform of electronic and atomic-scale modelling tools," *J. Phys. Condens. Matter*, vol. 32, no. 1, 2020, doi: 10.1088/1361-648X/ab4007.

[65] M. Brandbyge, J. L. Mozos, P. Ordejón, J. Taylor, and K. Stokbro, "Density-functional method for nonequilibrium electron transport," *Phys. Rev. B - Condens. Matter Mater. Phys.*, vol. 65, no. 16, pp. 1654011–16540117, 2002, doi: 10.1103/PhysRevB.65.165401.

[66] D. Stradi, U. Martinez, A. Blom, M. Brandbyge, and K. Stokbro, "General atomistic approach for modeling metal-semiconductor interfaces using density functional theory and nonequilibrium Green's function," *Phys. Rev. B*, vol. 93, no. 15, pp. 28–38, 2016, doi: 10.1103/PhysRevB.93.155302.

[67] J. P. Perdew, K. Burke, and M. Ernzerhof, "Generalized gradient approximation made simple," *Phys. Rev. Lett.*, vol. 77, no. 18, pp. 3865–3868, 1996, doi: 10.1103/PhysRevLett.77.3865.

[68] S. Grimme, J. Antony, S. Ehrlich, and H. Krieg, "A consistent and accurate ab initio parametrization of density functional dispersion correction (DFT-D) for the 94 elements H-Pu," *J. Chem. Phys.*, vol. 132, no. 15, 2010, doi: 10.1063/1.3382344.

[69] M. V. Bollinger, J. V. Lauritsen, K. W. Jacobsen, J. K. Nørskov, S. Helveg, and F. Besenbacher, "One-dimensional metallic edge states in MoS_2," *Phys. Rev. Lett.*, vol. 87, no. 19, pp. 3–6, 2001, doi: 10.1103/PhysRevLett.87.196803.

[70] J. V. Lauritsen *et al.*, "Size-dependent structure of MoS_2 nanocrystals," *Nat. Nanotechnol.*, vol. 2, no. 1, pp. 53–58, 2007, doi: 10.1038/nnano.2006.171.

[71] T. Markussen and K. Stokbro, "Metal-InGaAs contact resistance calculations from first principles," *Int. Conf. Simul. Semicond. Process. Devices, SISPAD*, pp. 373–376, 2016, doi: 10.1109/SISPAD.2016.7605224.

[72] V. Heine, "Theory of surface states," Phys. Rev., vol. 138, no. 6A, pp. 1689–1696, 1965, doi: 10.1103/PhysRev.138.A1689

[73] L. Jelver, D. Stradi, K. Stokbro, and K. W. Jacobsen, "Determination of Schottky barriers in 2D heterophase devices," arXiv:1911.09521v3, 2019.

[74] F. A. Padovani and R. Stratton, "Field and thermionic-field emission in Schottky barriers," *Solid State Electron.*, vol. 9, no. 7, pp. 695–707, 1966, doi: 10.1016/0038-1101(66)90097-9.

[75] Y. Guo, D. Liu, and J. Robertson, "3D Behavior of Schottky barriers of 2D transition-metal dichalcogenides," *ACS Appl. Mater. Interfaces*, vol. 7, no. 46, pp. 25709–25715, 2015, doi: 10.1021/acsami.5b06897.

[76] W. Mönch, *Semiconductor Surfaces and Interfaces* (Springer, Berlin, 2001).

[77] J. Tersoff, "Schottky barrier heights and the continuum of gap states," *Phys. Rev. Lett.*, vol. 52, pp. 465–568, 1984, doi: 10.1103/PhysRevLett.52.465

[78] C. Gong, L. Colombo, R. M. Wallace, and K. Cho, "The unusual mechanism of partial fermi level pinning at metal-MoS 2 interfaces," *Nano Lett.*, vol. 14, no. 4, pp. 1714–1720, 2014, doi: 10.1021/nl403465v.

[79] G. Hegde and R. Chris Bowen, "Effect of realistic metal electronic structure on the lower limit of contact resistivity of epitaxial metal-semiconductor contacts," *Appl. Phys. Lett.*, vol. 105, no. 5, 2014, doi: 10.1063/1.4892559.

[80] Q. Chen *et al.*, "Atomically flat zigzag edges in monolayer MoS_2 by thermal annealing," *Nano Lett.*, vol. 17, no. 9, pp. 5502–5507, 2017, doi: 10.1021/acs.nanolett.7b02192.

[81] A. Prakash, H. Ilatikhameneh, P. Wu, and J. Appenzeller, "Understanding contact gating in Schottky barrier transistors from 2D channels," *Sci. Rep.*, vol. 7, no. 1, pp. 1–9, 2017, doi: 10.1038/s41598-017-12816-3.

[82] J. Kang et al., "Graphene and beyond-graphene 2D crystals for next-generation green electronics," *Proc. SPIE*, 9083, 908305 (2014).

[83] C. Yeh, W. Cao, A. Pal, K. Parto, and K. Banerjee, "Area-selective-CVD technology enabled top-gated and scalable 2D-heterojunction transistors with dynamically tunable Schottky barrier," in *IEDM Tech. Dig.*, 2019, pp. 23.4.1–23.4.4, doi : 10.1109/IEDM19573.2019.8993600

[84] X. Ling *et al.*, "Parallel stitching of 2D materials," *Adv. Mater.*, vol. 28, no. 12, pp. 2322–2329, 2016, doi: 10.1002/adma.201505070.

[85] M. Zhao *et al.*, "Large-scale chemical assembly of atomically thin transistors and circuits," *Nat. Nanotechnol.*, vol. 11, no. 11, pp. 954–959, 2016, doi: 10.1038/nnano.2016.115.

[86] W. Hong, G. W. Shim, S. Y. Yang, D. Y. Jung, and S. Y. Choi, "Improved electrical contact properties of MoS_2-Graphene lateral heterostructure," *Adv. Funct. Mater.*, vol. 29, no. 6, pp. 1–8, 2019, doi: 10.1002/adfm.201807550.

[87] W. Cao, J. H. Chu, K. Parto, & K. Banerjee, "A mode-balanced reconfigurable logic gate built in a van der waals strata," *npj 2D Mater. Appl.*, vol. 5, no. 1, pp. 1-7, 2021, doi: 10.1038/s41699-020-00198-6.

[88] D. Zhang, C. Yeh, W. Cao, and K. Banerjee, "0.5T0.5R—An ultracompact RRAM cell uniquely enabled by van der waals heterostructures," *in IEEE Transactions on Electron Devices, vol. 68, no. 4, pp. 2033-2040, 2021,* doi: 10.1109/TED.2021.3057598.

[89] K. Parto, A. Pal, X. Xie, W. Cao, and K. Banerjee, "Interfacial thermal conductivity of 2D layered materials: An atomistic approach," in *IEDM Tech. Dig*., Dec. 2018, pp. 24.1.1–24.1.4.

[90] Y. Gong *et al.*, "Spatially controlled doping of two-dimensional SnS_2 through intercalation for electronics," *Nat. Nanotechnol.*, vol. 13, no. 4, pp. 294–299, 2018, doi: 10.1038/s41565-018-0069-3.

[91] R. Kappera *et al.*, "Phase-engineered low-resistance contacts for ultrathin MoS_2 transistors," *Nat. Mater.*, vol. 13, no. 12, pp. 1128–1134, 2014, doi: 10.1038/nmat4080.

[92] D. Saha and S. Mahapatra, "Anisotropic transport in 1T′ monolayer MoS_2 and its metal interfaces," *Phys. Chem. Chem. Phys.*, vol. 19, no. 16, pp. 10453–10461, 2017, doi: 10.1039/c7cp00816c

[93] K. Banerjee, S.C. Lin, A. Keshavarzi, S. Narendra, and V. De, "A self-consistent junction temperature estimation methodology for nanometer scale ICs with implications for performance and thermal management," In *IEEE International Electron Devices Meeting*, pp. 36-7, 2003, doi: 10.1109/IEDM.2003.1269421

[94] W. Liu, J. Kang, and Kaustav Banerjee, "Charactrization of $FeCl_3$ intercalation doped CVD few-layer graphene," *IEEE Electron Device Letters*, vol. 37, no. 9, pp. 1246 - 1249, Sept. 2016, doi: 10.1109/LED.2016.2597099.

[95] J. Jiang, J. Kang, W. Cao, X. Xie., H. Zhang. J.H. Chu, W. Liu, and K. Banerjee, "Intercalation doped multilayer-graphene-nanoribbons for next-generation interconnects," *Nano lett.*, vol. 17, no. 3, pp.1482-1488, 2017, doi.org/10.1021/acs.nanolett.6b04516

[96] J. Kang, Y. Matsumoto, X. Li et al., "On-chip intercalated graphene inductors for next-generation radio frequency electronics," *Nat Electron*, vol. 1 , no. 1, pp. 46–51, 2018, doi.org/10.1038/s41928-017-0010-z